Volume 4
Number 4
April 2025
Pages 463–590

Energy Advances

rsc.li/energy-advances

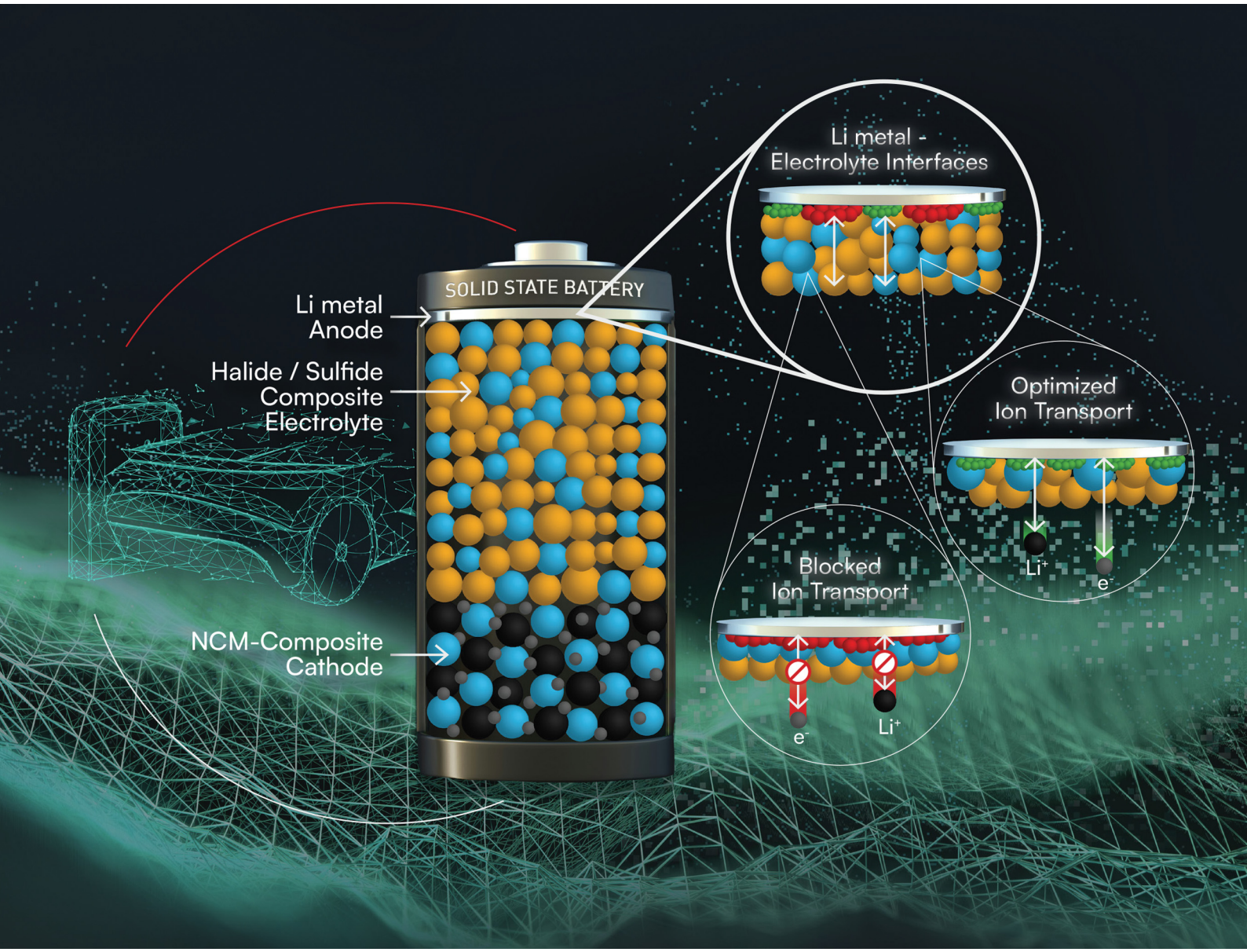

ISSN 2753-1457

ROYAL SOCIETY OF CHEMISTRY

PAPER
Artur Tron *et al.*
Insights into the chemical and electrochemical behavior of halide and sulfide electrolytes in all-solid-state batteries

Energy Advances

ROYAL SOCIETY OF CHEMISTRY

PAPER

View Article Online
View Journal | View Issue

Cite this: *Energy Adv.*, 2025, 4, 518

Insights into the chemical and electrochemical behavior of halide and sulfide electrolytes in all-solid-state batteries†

Artur Tron, *[a] Alexander Beutl,[a] Irshad Mohammad[a] and Andrea Paolella [ab]

Conventional lithium-ion batteries (LIBs) have become widely used in small and large applications, but the use of toxic and flammable liquid electrolytes can lead to safety issues and reduced cell performance. New generation solid-state lithium batteries (SSBs) have the potential to replace LIBs due to their safety and potentially high energy density (>450 W h kg^{-1}). The solid electrolyte (SE) is a crucial component in solid-state batteries. Among the available options, sulfide- and halide-based solid electrolytes stand out as promising candidates due to their high ionic conductivity and ease of processing. They are among the most prominent topics in solid electrolyte research for solid-state batteries. Despite their advantages like good compatibility with high-voltage cathodes and easy manufacturing, solid electrolytes still face issues of degradation of the Li metal/solid electrolyte interface. This is due to the formation of side reaction products at the interface, which inhibits lithium transport across it. The primary issue stems from the poor chemical and electrochemical stability of sulfide- and halide-based solid electrolytes when in contact with lithium metal. In this study, we have demonstrated that the composite electrolytes ($Li_3YCl_4Br_2$:Li_6PS_5Cl) comprising halide and argyrodite can prevent the formation of unfavorable interactions between the solid electrolyte and the Li metal anode. The Li/Li-symmetric cells employing the $Li_3YCl_4Br_2$:Li_6PS_5Cl electrolytes exhibited enhanced cycle life and high critical current density (CCD) from C/20 to C/2, compared to the symmetric cells utilizing only $Li_3YCl_4Br_2$ or Li_6PS_5Cl electrolyte. Furthermore, the Li/$Li_3YCl_4Br_2$/NCM half-cells demonstrated high initial coulombic efficiency and extended cycle life compared to half-cells utilizing traditional halide and argyrodite electrolytes. The approach described here offers a pathway to enhance halide-based solid-state batteries, providing a relatively simple and effective strategy.

Received 25th December 2024,
Accepted 1st February 2025

DOI: 10.1039/d4ya00618f

rsc.li/energy-advances

Introduction

Conventional lithium-ion batteries (LIBs) with liquid organic electrolytes have been commercialized for a wide range of applications, from small to large scale, and have become an integral part of daily life.[1,2] In recent decades, significant efforts have been made to replace conventional lithium-ion batteries with safer and more practical electrolyte systems. This includes exploring solid electrolytes, which function as both separators and electrolytes in the construction of solid-state batteries. Seen as a safer alternative to the flammable and toxic components in traditional liquid electrolytes, solid electrolytes are now a major focus in the research and development of various types of solid-state battery systems (SSBs).[3,4] Solid electrolyte systems offer several advantages over liquid systems. These include thermal, chemical, and electrochemical stability against lithium metal and cathode active materials, high ionic conductivity in the mS cm^{-1} range (which is close to that of liquid systems at 0.1 mS cm^{-1}), and low electronic conductivity (10^{-9}–10^{-10} mS cm^{-1}).[5,6] As a result, solid electrolyte systems are being considered as alternative candidates to replace liquid electrolytes.[7,8] Up to now, many solid electrolytes, such as polymers,[9] oxides of Li_2O–M_xO_y type,[10] NASICON,[11] perovskite,[12] garnet,[13] halides[14] and sulfides,[15] have been investigated for SSBs. Among the electrolyte types mentioned above, the sulfide or argyrodite-type Li_6PS_5X (X = Cl, Br, I) electrolyte demonstrates high ionic conductivity, stability with In/LiIn anodes, and favorable mechanical properties. These attributes have attracted significant research interest from both academic and industrial sectors.[15–17] However, the low electrochemical stability at high voltages (<4.1 V) of sulfide-based solid electrolytes remains an open question, as it limits the use of cathode materials, particularly those with high nickel content and lithium metal anodes. This is due to the formation of side reaction products, which ultimately

[a] *AIT Austrian Institute of Technology GmbH, Center for Transport Technologies, Battery Technologies, Giefinggasse 2, 1210 Vienna, Austria. E-mail: artur.tron@ait.ac.at*
[b] *Dipartimento di Scienze Chimiche e Geologiche Università degli Studi di Modena e Reggio Emilia Via Campi 103, Modena 41125, Italy*

† Electronic supplementary information (ESI) available. See DOI: https://doi.org/10.1039/d4ya00618f

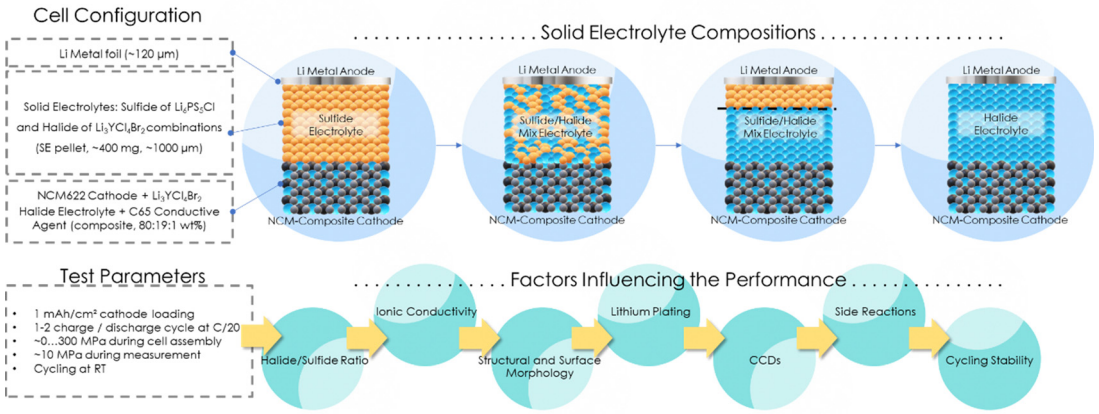

Fig. 1 Schematic outline for optimising a combination of halide and argyrodite solid electrolytes through dry-chemical processing and testing conditions.

contribute to capacity fading in the cell.[18–20] In recent years, several research groups have turned their attention to a promising alternative class of solid electrolytes: halide-based solid electrolytes with the formula Li_6MX_6 (where M^{3+} represents a metal, and X = Cl, Br, or I). These materials exhibit high ionic conductivity, are easier to synthesize, and offer enhanced chemical and thermal stability, especially against high-voltage cathodes and lithium metal.[20–23]

In order to overcome the challenges posed by the chemical instability and narrow electrochemical stability window of these electrolytes, we introduce the concept of a composite electrolyte for SSBs that combines the advantages of both sulfide and halide solid electrolytes. From the perspectives of thermodynamic, chemical, and electrochemical stability, particularly in relation to high-voltage cathodes and lithium metal, utilizing a composite electrolyte system may offer a more effective solution to address interface issues in solid-state batteries, which contributes to capacity fading.[24–26] Thus, incorporating sulfide electrolytes with halide electrolytes (Li_3InCl_6) between the cathode materials ($LiNi_{0.8}Co_{0.1}Mn_{0.1}O_2$ and $LiCoO_2$) and lithium metal leads to the stable cycling life of cells.[27–29] This type of approach is quite simple for improving the electrochemical performance of SSBs. However, it was shown that this combination can also lead to the formation of side products and capacity fading.[25,30] To address these challenges, numerous researchers have employed different methods to improve the electrochemical performance of SSBs using halide and sulfide electrolytes. These methods include using halide surface coatings for cathode materials,[31] introducing a sulfide interlayer between halide pellets,[32] and blending sulfide and halide electrolytes.[33] For SSB directions, we suggest that blending approaches between sulfide and halide solid electrolytes can play an important role in stabilizing the interface of the cathode and lithium metal anode, thereby reducing the formation of side reaction components.

Furthermore, as demonstrated in prior studies,[32,33] the combination of sulfide and halide electrolytes yields substantial chemical and electrochemical enhancements, leading to significant potential for utilizing this method as a surface agent to stabilize cathode and anode materials. It has been convincingly demonstrated that incorporating up to approximately 10 wt% of the halide phase into the sulfide phase mixture yields promising results. In this report, we discuss an application of blending sulfide and halide electrolytes in ratios of 80 : 20, 50 : 50, and 20 : 80 by weight, respectively. This is aimed at enhancing the interface stability and cycling performance of lithium metal anodes and NCM cathodes when combined with these electrolyte blends. In addition, it presents a simple design for investigating the impact of these combinations on the interface stability of sulfide and halide electrolytes, halide-based cathode composites, and lithium metal anodes (Fig. 1).

Experimental

Materials

Halide solid electrolyte powder ($Li_3YCl_4Br_2$, denoted as LYCB) was utilized in this work, which was kindly provided by Saint Gobain Recherche Paris (France). Commercially available Argyrodite material (Li_6PS_5Cl fine, denoted as LPSC) was purchased from NEI Corp. The polycrystalline powder $LiNi_{0.6}Co_{0.2}Mn_{0.2}O_2$ (denoted as NCM622) was used in this work, kindly provided by Umicore. These materials were used as received unless otherwise stated. Metallic lithium chips (15.6 mm in diameter, 0.25 mm thick) were purchased from MTI. The method used to prepare the lithium metal anode is described in ref. 34. The Li chips were cleaned before use by scraping off the surface layers with a scalpel. Subsequently, the cleaned lithium was further rolled in between two pouch foils (Dai Nippon Printing, D-EL408PH(3)S-250) using a glass cylinder. Thus, cleaned and smooth surfaces were obtained. Finally, electrodes of 10 mm diameter were cut from the prepared lithium using a manual punch.

Preparation blending halide and sulfide electrolyte

The prepared LPSC electrolyte was mixed with the LYCB electrolyte according to the weight percentage of 20 : 80, 50 : 50 and 80 : 20. The mixed electrolytes underwent grinding in a mortar and pestle for 20 min to obtain a uniform composition.

Material characterization

The crystalline phases of the pristine and blended electrolytes were determined by X-ray diffraction (XRD) analysis using a PANalytical X'Pert Pro diffractometer in Bragg–Brentano geometry with Cu Kα radiation (45 kV, 40 mA) in a 2θ range of 5–80° at a scan rate of 0.03° s^{-1}. The surface morphology of the samples was observed using field emission scanning electron microscopy (FE-SEM, ZEISS Supra 40) with energy-dispersive X-ray spectroscopy (EDS). The XPS spectra were calibrated using the standard adventitious C 1s peak at 284.8 eV. XPS spectra were analyzed using a nonlinear Shirley-type background. The core peaks and areas were fitted by a weighted least-squares fitting method using Lorentzian line shapes.

Preparation of electrolyte dry and bi-layer dry pellets

The process of making dry pellets with lithium metal is described in an earlier work.[35] Li|Li symmetric cells were assembled using densified electrolyte pellets as shown below (Fig. 2). The pellets were prepared in a few steps. First, around 400 mg of the pristine or blending powders was pressed into a ∅16 mm pellet with a 50 MPa pressure. Then the pressure was increased to 360 MPa for 5 min. After that, the lithium metal anode was then placed on both sides of the solid electrolyte pellet and transferred to a cell holder. A constant pressure of 10 MPa was applied on the cell during the electrochemical measurements.

Preparation of bi-layer dry pellets

The cathode composite was prepared in an Ar-filled glovebox (H_2O < 0.1 ppm; O_2 < 0.1 ppm). The cathode composite was prepared by manual mixing of NCM622, halide solid electrolyte (SE, LYCB), and conductive additive (CA, carbon black, Super C65, Imerys) together at a weight ratio of 80 : 19 : 1. The pressed cathode composite pellet at 50 MPa (loading of 1 mA h cm^{-2} and approximately 8–9 mg cm^{-2}) was placed on the solid electrolyte pellet (same method of preparation of electrolyte dry pellets as described above) from one side and compacted at a pressure of 300 MPa for 5 min. Next, the solid electrolyte pellet was sandwiched between lithium foil and a pressure of 10 MPa was applied during the electrochemical measurements.

Ionic conductivity of the dry pellets

Electrochemical impedance spectroscopy (EIS) measurements were performed in potentiostatic EIS (PEIS) mode with a frequency range from 2 MHz to 10 Hz and a voltage amplitude of 10 mV amplitude. This was done to assess the bulk ionic conductivity of the pristine and blending electrolytes in symmetrical cells with stainless steel (SS) blocking electrodes. The cells were tested at pressures ranging from 0 and 300 MPa to investigate the pressure-dependence behavior of the conductivity. The ionic conductivity of the electrolytes was then determined using a specific equation from a previous work.[34]

Electronic conductivity of dry pellets

The electronic conductivity of the solid electrolytes (SEs) was measured using a modified method based on a previously reported one.[36–38] The measurement involved applying stepwise voltages ranging from 100 to 500 mV, with increments of 100 mV, in a stainless steel (SS) blocking electrode/SE/blocking electrode cell setup. To follow the current responses in the cell, the cell voltage was held steady for 1 hour at each step. An exponential function was employed to analyze the relaxation behavior. The rapid decrease in current within the first 100 seconds was attributed to the ionic component of the conductivity, while the residual current was linked to electronic conductivity. The electronic conductivity of the solid electrolyte was determined from the slope of the voltammetric curve.

Lithium plating/stripping and CCD measurements

The tests were performed on symmetrical cells, and measurements were carried out in chronopotentiometric cyclic mode at a constant current density of 150 μA cm^{-2} for 1 hour for each half of the cycle. The area of the lithium metal and current collector discs is 0.785 cm^2. These tests provide information on cell polarization,[39] lithium deposition and dissolution kinetics,[40] and dendrite propagation.[41] The CCD was measured using different procedures, including step chronopotentiometry with current steps ranging from 0.01 mA cm^{-2} to 2.00 mA cm^{-2}. After each plating/stripping cycle, a potentiostatic impedance measurement (PEIS)

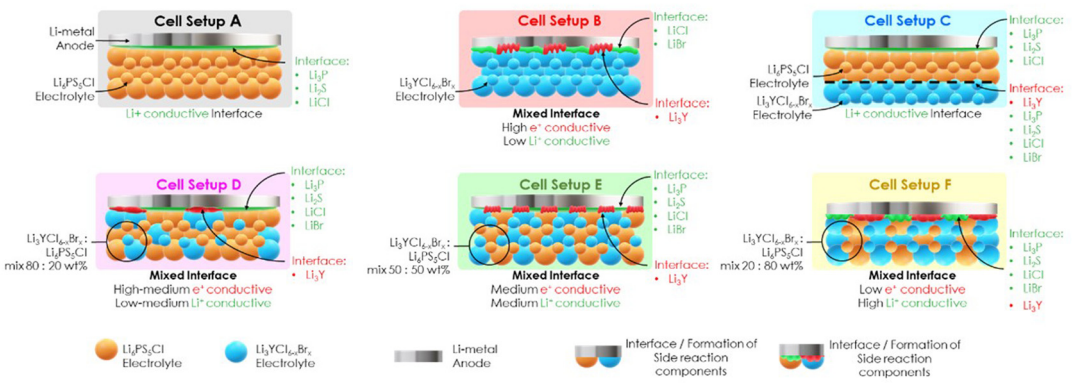

Fig. 2 Schematic of the different cell setups with different solid electrolyte combinations and lithium metal anode with the mixed electronic and ionic interface between the lithium metal anode and halide and sulfide electrolytes. Note: anode|separator|anode for dry pellets: cell setup A: Li|LPSC|Li; cell setup B: Li|LYCB|Li; cell setup C: Li|LPSC layer|LYCB|LPSC layer|Li; cell setup D: Li|LYCB: LPSC (80 : 20 wt%)|Li; cell setup E: Li|LYCB: LPSC (50 : 50 wt%)|Li; cell setup F: Li|LYCB: LPSC (20 : 80 wt%)|Li.

was conducted to check for possible short-circuiting of the cells due to dendrite formation. The PEIS was conducted from 2 MHz to 10 Hz using an AC excitation voltage of 50 mV.

Storage measurements

A storage test of Li|electrolyte|Li was performed using a pressurized device configuration at 10 MPa. This test utilized electrochemical impedance spectroscopy (EIS) ranging from 2 MHz to 10 Hz at a 10 mV amplitude in PEIS mode, conducted over a period of 30 days.

Electrochemical measurements

Galvanostatic cycling with potential limitation measurements was conducted using a Gamry Interface 1010 E. A current density of 0.05 mA cm^{-2} (C/20) was applied in the potential range of 4.3 V and 2.7 V (*vs.* Li/Li^+). Electrochemical impedance spectroscopy (EIS) was performed using the same equipment.

Results and discussion

In order to understand the issues related to the interface between solid electrolytes and the lithium metal anode, various types of cell setups with bi-layer solid electrolytes were used, as shown in Fig. 2. In this study, solid electrolytes such as sulfide Li_6PS_5Cl and halide $Li_3YCl_4Br_2$ and their combination were used as solid electrolyte layers in Li‖Li symmetric cell and Li‖NCM catholyte cell configurations (see Fig. S1 in ESI†). During the initial step of the analysis of bi-layers, we determined the ionic conductivity and density of these cell setups to understand the impact of these parameters on the electrochemical performance. The results are presented in the ESI† (Table S1 and Fig. S1). The powders used in the bi-layers were then evaluated by EIS measurements to assess the impact of layers on the ionic conductivity and densities (Fig. S2 and S3, ESI†). The powders were pelletized and sandwiched between lithium-ion blocking stainless steel (SS) electrodes in a setup with SS|solid electrolyte|SS cells. The Nyquist plot clearly shows the typical line, but the Z_{img} part was close to zero and did not contribute to the constant phase elements that were associated with the bulk or grain boundary resistance in the electrolyte related to the particle–particle contact area. It seems that interparticle contact has been reduced after adding the halide to sulfide powders into the SE pellet. As a result, we observed similar impedance and the same ionic conductivity values when compared to the pristine LYCB and combined samples of LPSC + LYCB. It is worth noting that cell setup F (LYCB : LPSC in a 20 : 80 wt% ratio) shows a slightly higher ionic conductivity compared to the other samples, which can be attributed to its mixed interface with low electronic conductivity and low lithium conductivity. Additionally, this may be linked to impurities formed during the mixing of sulfide and halide electrolytes. These impurities were observed in the XRD patterns as additional peaks, primarily located on the surface of the electrolyte particles. This led to high interfacial resistances (grain boundary), as previously reported.[39,40] On the other hand, cell setups A, C, D, and E show similar ionic conductivities (except the LPSC pristine). It is important to note that additional peaks for cell setup F can play an important role in the transport process and lead to the improvement of the interface. Moreover, the cell setup C (LYCB : LPSC (80 : 20 wt%)) shows a low ionic conductivity value of 0.6 mS cm^{-1} due to the high electronic conductivity and low lithium conductive mixed interface (Fig. 2). The cell setups A, B, C, D, E, and F exhibited ionic conductivity values at 25 °C and at 100 MPa that were similar to those reported in the literature, which are 1.4, 0.9, 0.6, 0.8, 0.8 and 1.5 mS cm^{-1}, respectively.[28,35] Additionally, the density of the as prepared pellets (densified at 300 MPa) for cell setups A, B, C, D, E, and F were 1.49, 2.42, 2.38, 2.28, 2.06 and 1.75 g cm^{-3}, respectively. These pellets were used for the ionic conductivity measurements. A significantly lower density was observed for the cell setup F compared to the other samples. Cell setup A (pristine LPSC powder) has a theoretical density of 1.64 g cm^{-3}, whereas cell setup B (pristine LYCB powder) has a theoretical density of 2.6 g cm^{-3} (ref. 42–44) (Table S1, ESI†). It should be noted that the mechanical properties (stability) of the obtained compositions might be significantly different when the halide electrolyte added to the sulfide mixture, particularly in terms of hardness and plasticity, compared to the pristine Li_6PS_5Cl and $Li_3YCl_4Br_2$ electrolytes. This is expected because of the influence of the impurity phases. Densification by cold-pressing might yield significant differences in the quality of the prepared powder pellets. As a consequence, samples with impurities appear to have a higher degree of defects and porosity. This could help to explain the lower ionic conductivities observed in samples with a high percentage (wt%) of halide electrolyte in the cell setups.

Previous studies have shown that incorporating elements into the structure of solid electrolytes or cathode/anode materials can induce lattice distortion and alter atomic occupancy. These changes can influence ionic conductivity through the microstrain effect.[45–47] Thus, to understand the microstrain effect of halide and sulfide mixtures in various cell setups and their influence on the structure of the samples affecting the lithium transport process, investigations were performed *via* the XRD, SEM, and XPS methods (Fig. 3). The diffraction peaks of the as-prepared pellets for cell setup A (pristine LPSC) match well with those for the lithium argyrodite Li_7PS_6 system (JCPDS No. 34-0688) belonging to the $F43m$ space group[18] (Fig. 3a). Whereas the X-ray diffraction patterns (Fig. 3a) for halide electrolytes indicate that the materials crystallize in two different phases, depending on the ratio between Cl and Br (cell setup B (pristine LYCB)): the Li_3YCl_6 sample crystallized in the trigonal $P3m1$[42] space group, similar to $Li_3YBr_xCl_{6-x}$ with $x = 2$. However, materials with $x > 2$, as well as the full bromide Li_3YBr_6, crystallized in the monoclinic $C2/m$[42] space group. For the samples with a high proportion of the LPSC phase, primarily in the lithium-argyrodite LPSC structure and with a reduced halide phase, examples include cell setups D, E, and F—comprising LYCB at weight ratios of 80 : 20, 50 : 50, and 20 : 80, respectively. Moreover, a lower amount of impurity phases (Li_2S, LiCl, and/or Li_3PO_4) was observed when a low halide ratio was used.[48] The additional phases indicate potential side reactions between sulfide and halide electrolytes, which can result in lower ionic conductivity

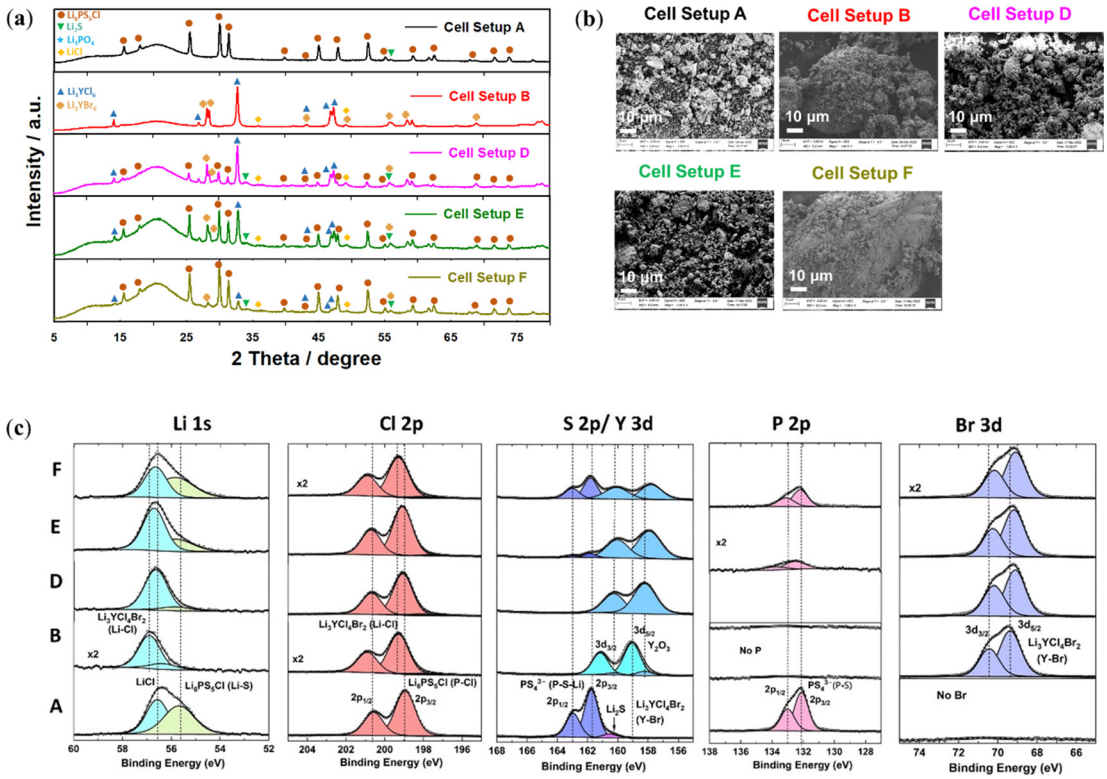

Fig. 3 (a) The XRD patterns, (b) the SEM images and (c) XPS analysis of the samples A, B, D, E and F. All the spectra were calibrated by adjusting the C 1s (C–C/C–H) peak at 284.8 eV.

and high resistance due to the formation of resistive interlayers at the grain boundaries.[18,44] The introduction of excess halide electrolyte into the composite can lead to impurities or side reactions. This can potentially create an additional impurity phase in the prepared compositions, but this effect has not been fully investigated yet. It is possible that the side reaction components have insulating properties, which can hinder lithium transport and increase the electronic transport, thus reducing the ionic conductivity.[44,48] For example, additional peaks at 40° were observed for the LPSC solid electrolyte, indicating the presence of a highly conductive phase (Table S1 and Fig. S2, ESI†). Peaks at 43° are associated with the low ionic conducting phase, exhibiting peak shifts and impurity peaks following the mixing of sulfides and halides. This phenomenon is similarly observed during the synthesis of sulfide-based solid electrolytes.[28,49,50] The SEM images show that there are small changes in the particle or grain size that lead to the formation of unwanted components (Fig. 3b). It should be noted that the pristine LPSC and LYCB electrolytes had a primary particle size of ~5 µm, while the LPSC:LYCB compositions have uniformly aggregated to form microsphere particles with a size in the range of ~15 µm. On the other hand, a decrease of Li_2S was observed when the amount of halide electrolyte in the sulfide electrolyte compositions increased from 20 to 80 wt%, as shown in Fig. S4 (EDS analysis, ESI†). When the surface area of contact between sulfide and halide decreases, successful lithium transport can be due to the formation of new interlayers, which are thinner compared to the samples with a high amount of halide.

The surface chemical compositions of the as-prepared sulfide, halide, and composted electrolytes were analyzed by XPS: Fig. 3c displays the XPS spectra of Li_6PS_5Cl (cell setup A), $Li_3YCl_4Br_2$ (cell setup B), and Li_6PS_5Cl:$Li_3YCl_4Br_2$ composite electrolytes (cell setups D–F). XPS was performed on each type of electrolyte to analyze the Li 1s, Cl 2p, S2 p, Y 3d, P 2p, and Br 3d regions. The high-resolution S 2p spectrum for sample A shows a doublet located at 161.7 (S $2p_{3/2}$) and 162.9 (S $2p_{1/2}$), ascribed to the PS_4^{3-} thiophosphate units of the Li_6PS_5Cl compound.[51] A second doublet has been detected at binding energies of 132.0 and 132.9 eV in the P 2p region, which can also be attributed to the PS_4^{3-} unit, confirming the presence of the sulfide electrolyte.[52] A trace of Li_2S was detected in the S 2p region at a binding energy of 160.4 eV, matching with the result from the XRD pattern (Fig. 3a).[53] In sample B, there is a doublet peak observed at 199.2 and 200.8 eV in the Cl 2p region, and another doublet in the Y 3d region observed at 159.0 and 161.1 eV.[28,54] Both doublets are attributed to the pure $Li_3YCl_4Br_2$ electrolyte. Additionally, Li 1s (56.8 eV) and Br 3d signals at 69.3 eV ($3d_{5/2}$) and 70.4 eV ($3d_{3/2}$) confirm the presence of $Li_3YCl_4Br_2$ electrolyte.[55] Interestingly, a small signal corresponding to Y_2O_3 is observed in the Y 3d region at 158.2 eV ($3d_{5/2}$) and 160.2 eV ($3d_{3/2}$), likely due to surface contamination of the sample during material handling.[56] The XPS measurements revealed signals corresponding to both electrolytes. It is important to highlight that, unlike XRD measurements, Li_2S was detected exclusively in cell setup A and not in other cell setups based on XPS spectra. This observation can be attributed to the composition

of cell setup A, which consists of a pure sulfide electrolyte. In contrast, other setups (D, E, and F) contain reduced sulfide phases due to the introduction of halide phases. A possible explanation for this phenomenon is that Li_2S phase particles may be covered by halide phases, rendering them undetectable by X-ray photoelectron spectroscopy (XPS). The signal intensities of the electrolytes were perfectly aligned with their compositions, demonstrating a precise correlation like in the XRD patterns. Y_2O_3 peaks with relatively high intensity are also observed in the composite electrolytes, indicating a surface contamination with moisture leading to oxide formation, like in the $Li_3YCl_4Br_2$ electrolyte case. Impurities like LiCl were detected at 56.5 eV in the Li 1s region) in almost every electrolyte composition, consistent with the XRD findings.[57]

There are many methods to determine the CCD of a solid electrolyte layer with the lithium metal anode, such as stepwise (step chronopotentiometry) or continuously (galvanodynamic polarization), and control parameters include current (charge-control) or time (time-control).[34,58] Before testing the cell setup configuration in a half cell with a cathode material, we first investigated the lithium plating and stripping study in the symmetric Li|electrolytes|Li cells to avoid the rate limitations and degradation of the cathode, and to understand the maximum applied current to these compositions (Fig. 4a and Table S2, ESI†). It was found that the LYCB pristine (cell setup B) maintains a higher critical current density at 1C compared to LPSC pristine (cell setup A, C/2). At the same time, the LYCB : LPSC (20 : 80 wt%) composition showed a high current density (C/2 with lower polarization values) compared to the 80 (2C with higher polarization values) and 50 (C/5) wt% of LYCB. This means that the critical current density values decrease with increasing halide electrolyte concentration in the sulfide compositions, which could be related to the formation of impurity phases at the grain boundaries hindering the lithium ion diffusion (Fig. 3). Furthermore, increasing the amount of halide phase in the sulfide compositions can lead to the formation of unwanted species with poor ionic conductive transport, like high insulating nature Li_2S, which could create inhomogeneous contact between the lithium and solid electrolyte. This can result in an irregular lithium ion flux distribution at the lithium metal anode and solid electrolyte interface, leading to lithium dendritic growth and low critical current density.[34,59] In addition, different particle sizes and densities between sulfide and halide electrolytes can result in an increase in the grain boundary resistance or interface resistance, which plays an important role in the formation of lithium dendrites that grow into solid electrolytes.[60,61] Based on the obtained data from CCD (Fig. 4a), we can conclude that cell setup F (20 wt% of halide) has smaller grain size and higher grain boundary resistance that is confirmed by the XRD

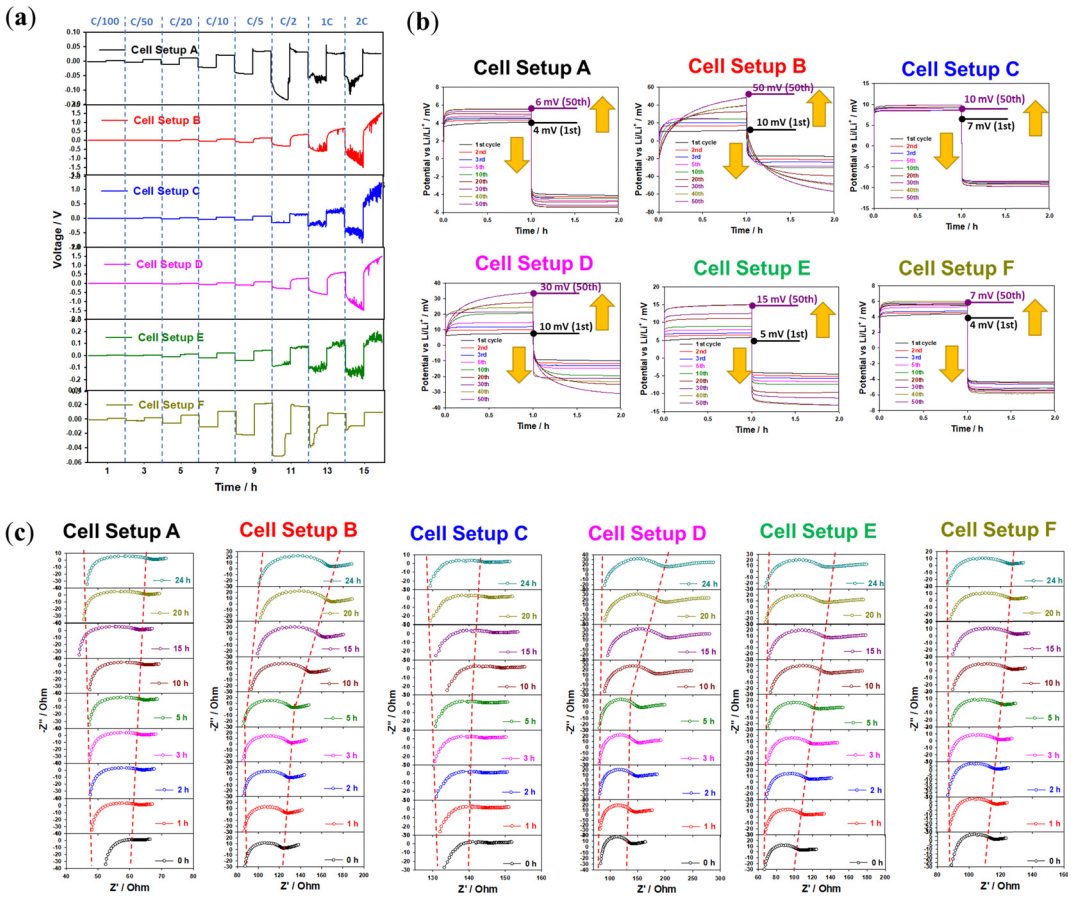

Fig. 4 (a) Critical current densities, (b) plating and stripping process at current densities of C/20, and (c) Nyquist plots at various storage times for 24 h of cell setup from Fig. 2 at various current densities.

(Fig. 3a) and ionic conductivity measurements (Table S1, ESI†). Fig. 4b shows the plating and stripping process during the long-term life of 50 cycles at C/20 (Table S3, ESI†). The pristine LPSC (cell setup A) maintains a stable plating and striping process with low polarization. In contrast, the pristine LYCB (cell setup B) demonstrated capacity fading due to the formation of side products. Moreover, halide electrolyte between two LPSC layers (cell setup C) shows behavior similar to the pristine LPSC (cell setup A), thanks to preventing the formation of side reaction components. However, in the case of the combined electrolyte (sulfide and halide) approach, the electrolyte degradation and capacity fading were especially observed for cell setups D and E. Although the polarization for cell setup F is quite low and similar to pristine LPSC, it could be due to the formation of stable SEI layer formation during the plating and stripping process. It is important to note that the low electronic and high ionic conductive mixed interface layer for cell setup F improves the transport of lithium between the lithium anode and solid electrolyte, leading to the uniform distribution of lithium ions into the solid electrolyte layer, and enhances the plating and striping process in general (Fig. 4b). In addition to the critical current density and plating/stripping measurements, we also examined the formation of the interphase product (increase resistance vs time) using EIS measurements over a 24 h period in contact with the lithium metal anode (Fig. 4c). After extending the contact time with the lithium metal anode to more than 24 hours, cell setup F demonstrates a stable interfacial resistance compared to cell setups B, D, and E. This stability is attributed to the formation of side reaction components, such as the Li_3Y alloy, which creates a layer with high electronic conductivity but low ionic conductivity, unlike the highly conductive layers formed by Li_3P, Li_2S, LiCl, and LiBr components.[28,62–66]

Fig. 5 presents the charge–discharge curves of all cell setups (A to F) in the voltage range of 2.7–4.3 V (*vs.* Li/Li^+) at the current density of C/20. The cell setup A (pristine Li_6PS_5Cl) shows a lower specific capacity (108 mA h g^{-1}) due to oxidation stability than LPSC but high stability against reduction of the simultaneous formation of L_2S, P_2S_5 and LiCl phase at the LPSC and NCM622 interface.[28,48] Whereas cell setup B (pristine halide) demonstrated a relatively higher capacity (150 mA h g^{-1}), thanks to the high oxidative stability of $Li_3YCl_4Br_2$ (>4.3 V *vs.* Li/Li^+).[21,42] In order to enhance the cyclability of the halide electrolyte-based cell, the LYCB electrolyte was sandwiched between two LPSC electrolyte layers (see cell setup C), which illustrated the specific capacity of 149 mA h g^{-1} due to the thin layer of LPSC which led to the formation of a stable anode interface. In addition, the total resistance of the demonstrated cell with the LPSC electrolyte is lower compared to the LYCB electrolyte (Fig. S5, ESI†). Cell setups D and E exhibit lower ionic conductivity compared to cell setup F, as the total resistance of the cell increases with a higher proportion of the halide phase. In the first cycle, cell setups D, E, and F show high initial specific charge/discharge capacities of 184/134, 163/125, and 176/130 mA h g^{-1}, with coulombic efficiencies of 98%, 96%, and 99%, respectively (Fig. 5a). These results also support the idea that the lower amount of halide phase (20 wt%) effectively reduces irreversible electrolyte decomposition or the occurrence of side reactions during the first cycle. It should be noted that the NCM622 cathode used in the cell setups showed quite similar electrochemical behaviour as it had in a non-aqueous electrolyte.[67] The stable discharge capacity of cell setup F (LYCB : LPSC = 20 : 80 wt%) can be attributed to the close solid–solid contact between the halide and sulfide electrolytes and the NCM cathode. This contact is facilitated by differences in the mechanical flexibility, density, and high ionic conductivity of the LYCB and LPSC electrolytes (Table S1, ESI†). After the first cycle, the side reaction of the cells was reduced and the coulombic efficiency for all cell setups A, B, D, E, and F reached over 93–99% and exhibited discharge capacity values of 107, 149, 146, 127, 116, and 126 mA h g^{-1} after the 2nd cycle, respectively (Fig. 5a and Table S4, ESI†). In addition, the electrochemical performance of combined halide and sulfide electrolytes, compared to pristine electrolyte layers, demonstrates a promising approach to enhancing the cycle life of cells with cathode materials. This is due to their effective prevention of lithium dendrite formation at low current densities, which can otherwise cause short-circuiting and capacity fading. Furthermore, this combined electrolyte approach reduces the use of the more toxic and environmentally harmful LPSC electrolyte in cell fabrication.

Although scientists are actively researching solid-state batteries to translate their academic findings into practical industrial applications, these batteries are not yet widely used. This is primarily due to their lower performance, complex processing, and the higher resistance of solid electrolytes compared to conventional liquid electrolytes, which limits their applications. Therefore, for the practical deployment of solid-state batteries, solid electrolytes must exhibit high ionic conductivity, low electronic conductivity, and electrochemical and chemical stability with respect to both the active materials and lithium metal.[4,8,68] Notably, the increase in electronic conductivity of solid electrolyte can be attributed to the different valences of components and the formation of side reaction components or impurity phases. Therefore, the presence of electronic conductivity in solid electrolytes impacts their performance due to their complex structures. Even a small increase in electronic conductivity can negatively affect solid-state batteries by leading to high self-discharge. For this reason, it is essential for the combination of halide and sulfide electrolytes to have very low electronic conductivity. Specifically, the electronic conductivity of these solid electrolytes must be at least five orders of magnitude lower than their ionic conductivity[8,37] for their successful application in SSB cells. The combination of halide and sulfide electrolytes (cell setups A, B, C, D, E and F) have ionic conductivity values of (1.4, 0.9, 0.6, 0.8, 0.8 and 1.5 mS cm^{-1}, respectively) (as shown in Table S1 and Fig. S2, ESI†) and low electronic conductivity (1.25×10^{-10}, 0.67×10^{-10}, 0.18×10^{-10}, 7.36×10^{-10}, 7.18×10^{-10} and 0.57×10^{-10} mS cm^{-1}, respectively) compared to glassy solid electrolytes such as LiPON, which have ionic conductivity ($\sim 10^{-4}$) and electronic conductivity ($\sim 10^{-13}$ mS cm^{-1}).[69,70] For calculation of the electronic conductivity of the solid electrolyte, we measured current–voltage dependencies, which exhibited

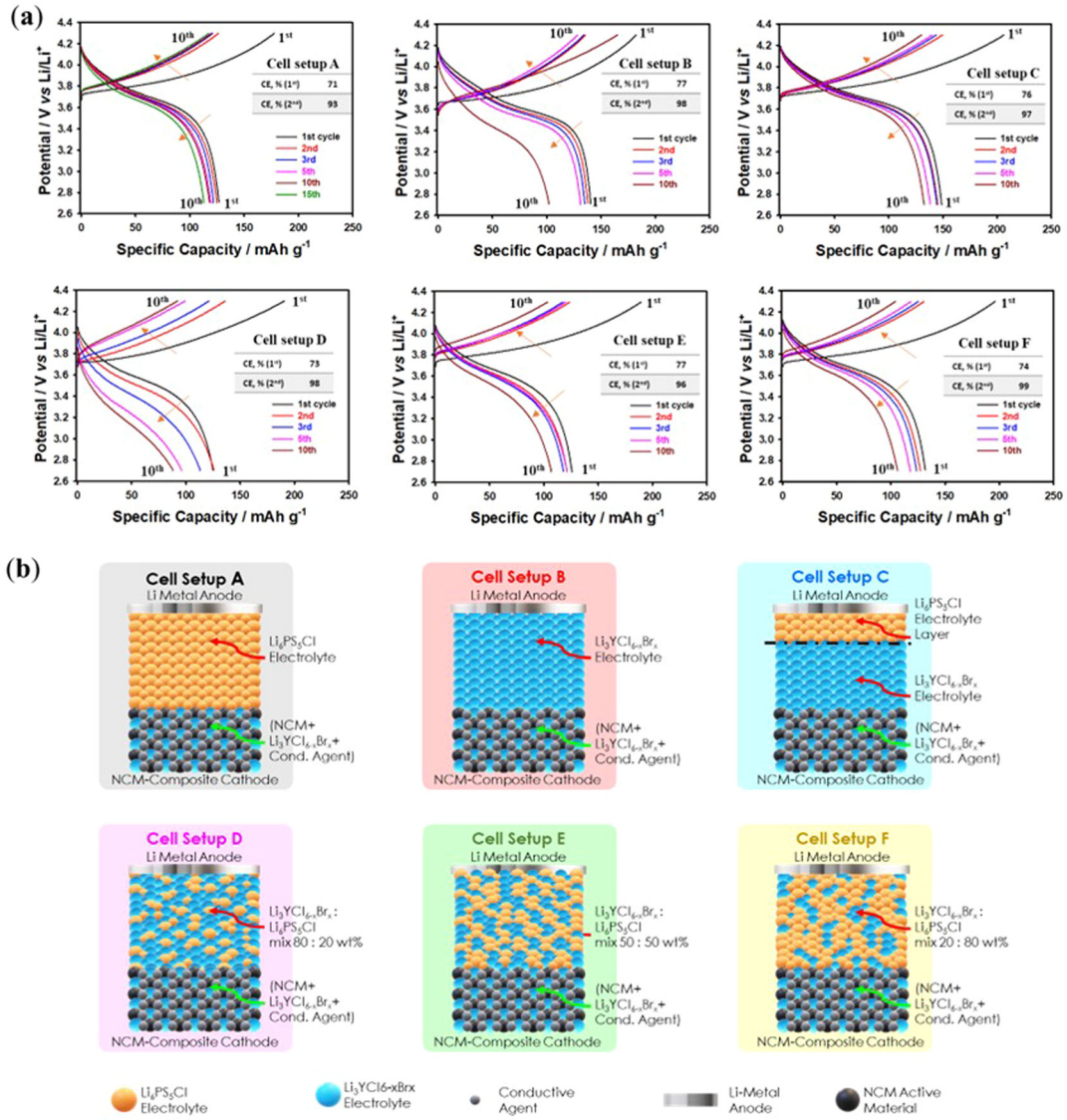

Fig. 5 (a) Charge and discharge curves of cell setups with the 1st and 2nd cycles at current densities of C/20 in the potential range of 2.7–4.3 V (*vs.* Li/Li^+). (b) Schematic of the different cell setups with different solid electrolyte combinations of halide and sulfide electrolytes, NCM622 cathode composite and lithium metal anode. Note: anode|separator|cathode for bi-layer dry pellets: cell setup A: Li|LPSC|NCM622 (+LYCB+C65); cell setup B: Li|LYCB|NCM622 (+LYCB+C65); cell setup C: Li|LPSC|LYCB|NCM622 (+LYCB+C65); cell setup D: Li|LYCB : LPSC (80 : 20 wt%)|NCM622 (+LYCB+C65); cell setup E: Li|LYCB : LPSC (50 : 50 wt%)|NCM622 (+LYCB + C65); cell setup F: Li|LYCB : LPSC (20 : 80 wt%)|NCM622(+LYCB+C65).

a linear character. In Fig. S6 (ESI†), Ohm's law was used to calculate the electronic conductivity from their slopes of the straight lines. The current–voltage characteristics of the solid electrolytes were determined using a cell with blocking electrodes (stainless steel). Note that the significant scatter in the data obtained is related to the low current value through the system. Based on the obtained results, the electrochemical performance of SSB cells was improved by using a combination of halide and sulfide electrolytes due to the high ionic and low electronic conductivity of the solid electrolyte combination layer. Therefore, these combinations of halide/sulfide solid electrolyte layers are promising candidates for their use as solid electrolytes with high energy density cathodes and a lithium anode in solid state batteries. In the case of combined halide and sulfide electrolyte, the uniform formation of a layer on the surface of the lithium metal anode surface prevents unwanted reactions and allows the cell setups of B and C to have higher specific capacity and better cycling stability at high charge cut-off potentials compared to the cell setup of A, D, E and F (Fig. 2). Thus, it has been demonstrated that the formation of "friendly" conductive side reaction components with high ionic and low electronic conductivity, along with significantly higher chemical and electrochemical stability towards lithium metal, leads to improved electrochemical performance and lower electrode resistance when a combination of halide and sulfide electrolytes (cell setup of F) is used in contact with NCM622 and a lithium metal anode (Fig. S5, ESI†). It should be noted that these combinations of electrolytes can produce and form side reaction components (Fig. 2), resulting in mixed electronic and ionic conductive layers, which may influence and ensure slow or fast kinetics for interfacial charge transfer,

ultimately leading to the prevention of lithium buildup between the lithium anode and solid electrolyte interface (Fig. 5). For this reason, the diffusion coefficient of the cell setups of A, B, C, D, E and F was calculated after cycling and found to be 4.08×10^{-20}, 7.79×10^{-20}, 1.23×10^{-19}, 1.04×10^{-20}, 2.23×10^{-20} and 5.27×10^{-20} cm^2 s^{-2}, respectively.[71] Among all the cell configurations, cell setups C and F have a higher diffusion coefficient than the others, indicating efficient lithium transport during cycling. This leads to improved rate capability, a stable SEI (side reaction component) layer on the surface, and better reversible exchange reactions. Furthermore, cell setups C and F demonstrate higher chemical diffusion factors compared to pure halide electrolytes, which correlate with more stable and superior cycling performance.[28] Cell setups C and F, when in contact with the lithium metal, maintained their intimate contact during the cycle life, as shown in Fig. S7 (ESI†). However, in cell setups D and E, the morphology of the lithium metal anode changed significantly, and the interfacial layer has different combinations of a mixed electronic and ionic interface between the lithium metal anode and halide and sulfide electrolytes, suggesting that the slow and fast lithium-ion transport can have an impact on the cycling results (Fig. 5).

A combination of different solid electrolytes can improve the interface between the cathode material and the lithium metal anode, resulting in stable electrochemical performance without altering the charge–discharge mechanisms (Fig. S8, ESI†). To better assess the contribution of the electrode material's capacity, the cycling test was performed on cells in the SS electrode configuration. The results showed that these combinations of halides and sulfides did not contribute to the active material's capacity. Instead, most of them were associated with the formation of conductive phases, which impacted the stability of the lithium metal and contributed to capacity degradation, as shown in Fig. S7 (ESI†). In addition, the specific discharge capacity of the coated SS electrode at the level of 0.025 μA h cm^{-2} is negligible compared to the NCM622 active material (Fig. 5). The practical capacity of the pristine NCM622 is 170 mA h g^{-1},[67] and the obtained specific capacity of the NCM622 cathode in the non-aqueous liquid electrolyte in contact with the lithium metal anode is shown in Fig. S9 (ESI†). Based on the discharge capacities of the cells, it is possible to assume that the presence of side reaction components on the surface of the SS electrode, formed during cycling at a lower potential of 2.7 V, is due to the decomposition potential of the components of the aqueous electrolytic solution being lower than 1 V,[37] while the decomposition of the components of the combination electrolytic solution is not detected. The data show that during SSB operation in the voltage range of 1.0–4.3 V (*vs.* Li/Li^+), the cell setups demonstrate a high electrochemical stability window. No significant electrochemical processes were observed on the surface of the SS electrode. However, cell setups containing a larger amount of sulfide Li_6PS_5Cl electrolyte demonstrate a slightly higher specific capacity. This increase may be attributed to certain solid electrolyte (glassy) materials, which show potential as both cathode and anode materials for lithium-ion batteries. These materials feature well-controlled internal structures that facilitate lithium ion conduction, resulting in enhanced specific capacities.[72,73]

Conclusions

This work has shown that the combination of halide and argyrodite solid electrolytes can prevent the formation of unfavourable interactions between the solid electrolyte and the lithium metal anode. An ionic conductivity of 1.5 mS cm^{-1} was obtained for the optimized compositions incorporating the halide phase into the sulfide composition. Morphological analysis revealed that a combination of LYCB and LPSC acts as a flux that can limit particle aggregation during mixing with the formation of relevant interlayers (thin layers compared to samples with a high amount of halide) for successful lithium transport with minimal impact on the electronic process. The combination of halide and argyrodite in the Li/Li-symmetric cell can provide cycle life stabilization and increase the high critical current density (CCD) from C/20 to C/2 compared to the pure halide and argyrodite electrolytes. In addition, when combined with a half Li/NCM cell, the interfacial layer in the lithium/electrolyte and electrolyte/cathode interfaces can maintain a high initial coulombic efficiency and cycle life compared to the original halide and argyrodite electrolytes. This approach to the improvement of halide SSBs can be a relatively simple and efficient strategy to implement.

Author contributions

Conceptualization: [Artur Tron, Alexander Beutl], methodology: [Artur Tron, Alexander Beutl], general experimental investigation and electrochemical analysis: [Artur Tron, Alexander Beutl], characterization XRD: [Raad Hamid], characterization SEM: [Susan Montes], characterization XPS: [Irshad Mohammad], writing – original draft preparation: [Artur Tron, Alexander Beutl], writing – review and editing: [Artur Tron, Alexander Beutl, Irshad Mohammad, Andrea Paolella].

Data availability

The data supporting this study's findings are available from **https://nextcloud.ait.ac.at/index.php/s/Nr4GmBEwS7boXYa** (PW: 2775541290).

Conflicts of interest

The authors have no relevant financial or non-financial interests to declare. The authors have no conflicts of interest to declare that are relevant to the content of this article. All authors certify that they have no affiliations with or involvement in any organization or entity with any financial interest or non-financial interest in the subject matter or materials discussed in this manuscript. The authors have no financial or proprietary interests in any material discussed in this article.

Acknowledgements

This work was supported by the financial support of the Austrian Federal Ministry for Climate Action, Environment, Energy, Mobility, Innovation, and Technology. The presented work was supported by the European Union's Horizon Europe programme for research and innovation under grant agreement no. 101069681 (HELENA project). Furthermore, the authors want to express their gratitude to Susan Montes for the SEM/EDS analysis of the samples and Raad Hamid for the XRD measurements of the obtained samples.

References

1 J. B. Goodenough and Y. Kim, Challenges for rechargeable Li batteries, *Chem. Mater.*, 2009, **22**, 587–603.
2 G. B. Xia, L. Cao and G. L. Bi, A review on battery thermal management in electric vehicle application, *J. Power Sources*, 2017, **367**, 90–105.
3 Y. Horowitz, C. Schmidt, D. H. Yoon, L. M. Riegger, L. Katzenmeier, G. M. Bosch, M. Noked, Y. Ein-Eli, J. Janek, W. G. Zeier, C. E. Diesendruck and D. Golodnitsky, Between liquid and all solid: A prospect on electrolyte future in lithium-ion batteries for electric vehicles, *Energy Technol.*, 2020, **8**(11), 2000580.
4 Y. Meesala, A. Jena, H. Chang and R.-S. Liu, Recent Advancements in Li-Ion Conductors for All-Solid-State Li-Ion Batteries, *ACS Energy Lett.*, 2017, **2**(12), 2734–2751.
5 Z. Zhang, Y. Shao, B. Lotsch, Y.-S. Hu, H. Li, J. Janek, L. F. Nazar, C.-W. Nan, J. Maier, M. Armand and L. Chen, New horizons for inorganic solid state ion conductors, *Energy Environ. Sci.*, 2018, **11**, 1945–1976.
6 Y. He, Y. Dong, L. Qiao, C. M. Costa, S. Lanceros-Mendez, J. Han and W. He, Recent progress in ultra-thin solid polymeric electrolytes for next-generation lithium batteries, *Energy Storage Mater.*, 2024, **67**, 103329.
7 Q. Wang, Y. Zhou, X. Wang, H. Guo, S. Gong, Z. Yao, F. Wu, J. Wang, S. Ganapathy, X. Bai, B. Li, C. Zhao, J. Janek and M. Wagemaker, Designing lithium halide solid electrolytes, *Nat. Commun.*, 2024, **15**, 1050.
8 A. Tron, Insight of transport properties of glassy solid electrolytes for energy storage applications, *Solid State Sci.*, 2024, **153**, 107556.
9 Q. Jiang, A. Beutl, H. Kühnelt and A. Bismarck, Structural composite batteries made from carbon fibre reinforced electrodes/polymer gel electrolyte prepregs, *Compos. Sci. Technol.*, 2023, **244**, 110312.
10 A. Tron, A. Nosenko, Y. D. Park and J. Mun, The solid electrolytes Li_2O–LiF–Li_2WO_4–B_2O_3 with enhanced ionic conductivity for lithium-ion battery, *J. Ind. Eng. Chem.*, 2019, **73**, 62–66.
11 Y. Deng, C. Eames, B. Fleutot, R. David, J.-N. Chotard, E. Suard, C. Masquelier and M. Saiful Islam, Enhancing the lithium ion conductivity in lithium superionic Conductor (LISICON) solid electrolytes through a mixed polyanion effect, *ACS Appl. Mater. Interfaces*, 2017, **8**, 7050–7058.
12 J. Lu and Y. Li, Perovskite-type Li-ion solid electrolytes: a review, *J. Mater. Sci.: Mater. Electron.*, 2021, **32**, 9736–9754.
13 C. Wang, K. Fu, S. P. Kammampata, D. W. McOwen, A. J. Samson, L. Zhang, G. T. Hitz, A. M. Nolan, E. D. Wachsman, Y. Mo, V. Thangadurai and L. Hu, Garnet-type solid-state electrolytes: materials, interfaces, and batteries, *Chem. Rev.*, 2020, **120**, 4257–4300.
14 J. Liang, X. Li, J. T. Kim, X. Hao, H. Duan, R. Li and X. Sun, Halide layer cathodes for compatible and fast-charged halides-based all-solid-state Li metal batteries, *Angew. Chem., Int. Ed.*, 2023, **62**, e20221708.
15 Y.-T. Chen, J. Jang, J. A. S. Oh, S.-Y. Ham, H. Yang, D.-J. Lee, M. Vicencio, J. B. Lee, D. H. S. Tan, M. Chouchane, A. Cronk, M.-S. Song, Y. Yin, J. Qian, Z. Chen and Y. S. Meng, Enabling uniform and accurate control of cycling pressure for all-solid-state batteries, *Adv. Energy Mater.*, 2024, 2304327.
16 K. J. Kim, M. Balaish, M. Wadaguchi, L. Kong and J. L. M. Rupp, Solid-state Li–metal batteries: challenges and horizons of oxide and sulfide solid electrolytes and their interfaces, *Adv. Energy Mater.*, 2021, **11**, 2002689.
17 K. T. Kim, T. Y. Kwon and Y. S. Jung, Scalable fabrication of sheet-type electrodes for practical all-solid-state batteries employing sulfide solid electrolytes, *Curr. Opin. Electrochem.*, 2022, **34**, 101026.
18 R. Koerver, I. Aygün, T. Leichtweiß, C. Dietrich, W. Zhang, J. O. Binder, P. Hartmann, W. G. Zeier and J. Janek, Capacity fade in solid-state batteries: Interphase formation and chemomechanical processes in Nickel-rich layered oxide cathodes and lithium thiophosphate solid electrolytes, *Chem. Mater.*, 2017, **29**, 5574.
19 C. Doerrer, I. Capone, S. Narayanan, J. Liu, C. R. M. Grovenor, M. Pasta and P. S. Grant, High energy density single-crystal NMC/Li_6PS_5Cl cathodes for all-solid-state lithium-metal batteries, *ACS Appl. Mater. Interfaces*, 2021, **13**(31), 37809–37815.
20 K. Kim, D. Park, H.-G. Jung, K. Y. Chung, J. H. Shim, B. C. Wood and S. Yu, Materials design strategy for halide solid electrolytes for all-solid state high-voltage Li-ion batteries, *Chem. Mater.*, 2021, **33**(10), 3669–3677.
21 C. Wang, J. Liang, J. T. Kim and X. Sun, Prospects of halide-based all-solid-state batteries: From material design to practical application, *Sci. Adv.*, 2022, **8**, eadc9516.
22 Y. Tanaka, K. Ueno, K. Mizuno, K. Takeuchi, T. Asano and A. Sakai, New oxyhalide solid electrolytes with high lithium ionic conductivity >10 mS cm for all-solid-state batteries, *Angew. Chem., Int. Ed.*, 2023, **62**, e202217581.
23 K. Wang, Q. Ren, Z. Gu, C. Duan, J. Wang, F. Zhu, Y. Fu, J. Hao, J. Zhu, L. He, C.-W. Wang, Y. Lu, J. Ma and C. Ma, A cost-effective and humidity-tolerant chloride solid electrolyte for lithium batteries, *Nat. Commun.*, 2021, **12**, 4410.
24 C. Rosenbach, F. Walther, J. Ruhl, M. Hartmann, T. A. Hendriks, S. Ohno, J. Janek and W. G. Zeier, Visualizing the chemical incompatibility of halide and sulfide-based electrolytes in solid-state batteries, *Adv. Energy Mater.*, 2023, **13**, 2203673.
25 T. Koç, F. Marchini, G. Rousse, R. Dugas and J.-M. Tarascon, In the search for the best solid electrolyte-layered oxide pairing for assembling practical all-solid-state batteries, *ACS Appl. Energy Mater.*, 2021, **12**, 13575–13585.

26 D. Park, H. Park, Y. Lee, S.-O. Kim, H.-G. Jung, K. Y. Chung, J. H. Shim and S. Yu, Theoretical design of lithium chloride superionic conductors for all-solid-state high-voltage lithium-ion batteries, *ACS Appl. Mater. Interfaces*, 2020, **12**, 34806–34814.

27 X. Li, J. Liang, N. Chen, J. Luo, K. R. Adair, C. Wang, M. N. Banis, T. Sham, L. Zhang, S. Zhao, S. Lu, H. Huang, R. Li and X. Sun, Water-mediated synthesis of a superionic halide solid electrolyte, *Angew. Chem., Int. Ed.*, 2019, **58**, 16427–16432.

28 C. Wang, J. Liang, J. Luo, J. Liu, X. Li, F. Zhao, R. Li, H. Huang, S. Zhao, L. Zhang, J. Wang and X. Su, A universal wet-chemistry synthesis of solid-state halide electrolytes for all-solid-state lithium–metal batterie, *Sci. Adv.*, 2021, **7**, eabh1896.

29 H. Zhang, Z. Yu, J. Cheng, H. Chen, X. Huang and B. Tian, Halide/sulfide composite solid-state electrolyte for Li-anode based all-solid-state batteries, *Chin. Chem. Lett.*, 2023, **34**, 108228.

30 T. Koç, M. Hallot, E. Quemin, B. Hennequart, R. Dugas, A. M. Abakumov, C. Lethien and J.-M. Tarascon, Toward optimization of the chemical/electrochemical compatibility of halide solid electrolytes in all-solid-state batteries, *ACS Energy Lett.*, 2022, **7**, 2979–2987.

31 J. S. Kim, S. Jung, H. Kwak, Y. Han, S. Kim, J. Lim, Y. M. Lee and Y. S. Jung, Synergistic halide-sulfide hybrid solid electrolytes for Ni-rich cathodes design guided by digital twin for all-solid-State Li batteries, *Energy Storage Mater.*, 2023, **55**, 193–204.

32 W. Ji, D. Zheng, X. Zhang, T. Ding and D. Qu, A kinetically stable anode interface for Li_3YCl_6-based all-solid-state lithium batteries, *J. Mater. Chem. A*, 2021, **9**, 15012–15018.

33 Y. Subramanian, R. Rajagopal and K.-S. Ryu, Blending a Li_3N/Li_3YCl_6 solid electrolyte with Li_6PS_5Cl argyrodite structure to improve interface stability and electrochemical performance in Lithium solid-state batteries, *J. Alloys Compd.*, 2023, **940**, 168867.

34 A. Tron, A. Orue, P. López-Aranguren and A. Beutl, Critical current density measurements of argyrodite Li_6PS_5Cl solid electrolyte at ambient pressure, *J. Electrochem. Soc*, 2023, **170**, 100525.

35 A. Beutl, A. Orue, P. López-Aranguren, A. I. P. Martinez, M. H. Braga, V. Kekkonen and A. Tron, Round-robin test of all-solid-state battery with sulfide electrolyte assembly in coin-type cell configuration, Electrochem, *Sci. Adv.*, 2024, e2400004.

36 F. Vereda, R. B. Goldner, T. E. Haas and P. Zerigian, Rapidly grown IBAD LiPON films with high Li-ion conductivity and electrochemical stability, *Electrochem. Solid-State Lett.*, 2002, **5**, A239–A241.

37 M. Menetrier, A. Lavasseur and P. Hagenmuller, Electrochemical properties of B_2S_3–Li_2S–LiI vitreous electrolytes, *J. Electrochem. Soc.*, 1984, **131**, 1971–1973.

38 A. Tron, A. Nosenko, Y. D. Park and J. Mun, Synthesis of the solid electrolyte Li_2O–LiF–P_2O_5 and its application for lithium-ion batteries, *Solid State Ionics*, 2017, **308**, 40–45.

39 G. Bieker, M. Winter and P. Bieker, Electrochemical in situ investigations of SEI and dendrite formation on the lithium metal anode, *Phys. Chem. Chem. Phys.*, 2015, **17**, 8670–8679.

40 K. N. Wood, E. Kazyak, A. F. Chadwick, K.-H. Chen, J.-G. Zhang, K. Thornton and N. P. Dasgupta, Dendrites and pits: untangling the complex behavior of lithium metal anodes through operando video microscopy, *ACS Cent. Sci.*, 2016, **2**(11), 790–801.

41 D. K. Singh, A. Henss, B. Mogwitz, A. Gautam, J. Horn, T. Krauskopf, S. Burkhardt, J. Sann, F. H. Richter and J. Janek, Li_6PS_5Cl microstructure and influence on dendrite growth in solid-state batteries with lithium metal anode, *Cell Rep. Phys. Sci.*, 2022, **3**, 101043.

42 E. van der Maas, W. Zhao, Z. Cheng, T. Famprikis, M. Thijs, S. R. Parnell, S. Ganapathy and M. Wagemaker, Investigation of structure, ionic conductivity, and electrochemical stability of halogen substitution in solid-state ion conductor $Li_3YBr_xCl_{6-x}$, *J. Phys. Chem. C*, 2023, **127**(1), 125–132.

43 C. Sedlmeier, T. Kutsch, R. Schuster, L. Hartmann, R. Bublitz, M. Tominac, M. Bohn and H. A. Gasteiger, From powder to sheets: A comparative electrolyte study for slurry-based processed solid electrolyte/binder-sheets as separators in all-solid-state batteries, *J. Electrochem. Soc.*, 2022, **169**, 070508.

44 A. Tron, A. Paolella and A. Beutl, New insights of infiltration process of argyrodite Li_6PS_5Cl solid electrolyte into conventional lithium-ion electrodes for solid-state batteries, *Batteries*, 2023, **9**(10), 503.

45 E.-J. Lee, Z. Chen, H.-J. Noh, S. C. Nam, S. Kang, D. H. Kim, K. Amine and Y.-K. Sun, Development of microstrain in aged lithium transition metal oxides, *Nano Lett.*, 2014, **14**, 4873–4880.

46 A. R. Symington, M. Molinari, J. A. Dawson, J. M. Statham, J. Purton, P. Canepa and S. C. Parker, Elucidating the nature of grain boundary resistance in lithium lanthanum titanate, *J. Mater. Chem. A*, 2021, **9**, 6487.

47 J.-F. Wu and X. Guo, Origin of the low grain boundary conductivity in lithium ion conducting perovskites: $Li_{3x}La_{0.67-x}TiO_3$, *Phys. Chem. Chem. Phys.*, 2017, **19**, 5880–5887.

48 D. H. S. Tan, E. A. Wu, H. Nguyen, Z. Chen, M. A. T. Marple, J. M. Doux, X. Wang, H. Yang, A. Banerjee and Y. S. Meng, Elucidating reversible electrochemical redox of Li_6PS_5Cl solid electrolyte, *ACS Energy Lett.*, 2019, **4**, 2418–2427.

49 R. Rajagopal, Y. Subramanian, S. Kang, J. Park and K.-S. Ryu, Improved interfacial stability of all-solid-state batteries using cation-anion co-doped glass electrolytes, *Commun. Mater.*, 2024, **5**, 78.

50 R. Rajagopal, Y. Subramanian, Y. J. Jung, S. Kang and K.-S. Ryu, Preparation of metal-oxide-doped $Li_7P_2S_8Br_{0.25}I_{0.75}$ solid electrolytes for all-solid-state lithium batteries, *ACS Appl. Mater. Interfaces*, 2023, **15**, 21016–21026.

51 J. Auvergniot, A. Cassel, J. B. Ledeuil, V. Viallet, V. Seznec and R. Dedryvere, Interface stability of argyrodite Li_6PS_5Cl toward $LiCoO_2$, $LiNi_{1/3}Co_{1/3}Mn_{1/3}O_2$, and $LiMn_2O_4$ in bulk all-solid-state batteries, *Chem. Mater.*, 2017, **29**, 3883–3890.

52 T. Swamy, X. Chen and Y.-M. Chiang, Electrochemical redox behavior of Li ion conducting sulfide solid electrolytes, *Chem. Mater.*, 2019, **31**(3), 707–713.

53 S. Ohno, R. Koerver, G. Dewald, C. Rosenbach, P. Titscher, D. Steckermeier, A. Kwade, J. Janek and W. G. Zeier,

Observation of chemomechanical failure and the influence of cut off potentials in all-solid-state Li–S batteries, *Chem. Mater.*, 2019, **31**, 2930–2940.

54 X. Wang, Z. Yang, N. Li, K. Wu, K. Gao, E. Zhao, S. Han and W. Guo, Influence mechanism of interfacial oxidation of Li_3YCl_6 solid electrolyte on reduction potential, *Chemistry*, 2024, **30**(20), e202303884.

55 J. Peng, L. Xian and L. B. Kong, Effects of Br substitution to improve the ionic conductivity of chloride electrolytes without changing crystal structure, *Ionics*, 2023, **29**, 2657–2664.

56 G. Xu, L. Luo, J. Liang, S. Zhao, R. Yang, C. Wang, T. Yu, L. Wang, W. Xiao, J. Wang, J. Yu and X. Sun, Origin of high electrochemical stability of multi-metal chloride solid electrolytes for high energy all-solid-state lithium-ion batteries, *Nano Energy*, 2022, **92**, 106674.

57 J. Auvergniot, A. Cassel, D. Foix, V. Viallet, V. Seznec and R. Dedryvère, Redox activity of argyrodite Li_6PS_5Cl electrolyte in all-solid-state Li-ion battery: An XPS study, *Solid State Ionics*, 2017, **300**, 78–85.

58 J. A. Lewis, C. Lee, Y. Liu, S. Y. Han, D. Prakash, E. J. Klein, H.-W. Lee and M. T. McDowell, Role of areal capacity in determining short circuiting of sulfide-based solid-state batteries, *ACS Appl. Mater. Interfaces*, 2022, **14**(3), 4051–4060.

59 D. K. Singh, A. Henss, B. Mogwitz, A. Gautam, J. Horn, T. Krauskopf, S. Burkhardt, J. Sann, F. H. Richter and J. Janek, Li_6PS_5Cl microstructure and influence on dendrite growth in solid-state batteries with lithium metal anode, *Cell Rep. Phys. Sci.*, 2022, **3**, 101043.

60 S. Yu and D. J. Siegel, Grain boundary contributions to Li-ion transport in the solid electrolyte $Li_7La_3Zr_2O_{12}$ (LLZO), *Chem. Mater.*, 2017, **29**, 9639–9647.

61 R. Raj and J. Wolfenstine, Current limit diagrams for dendrite formation in solid-state electrolytes for Li-ion batteries, *J. Power Sources*, 2017, **343**, 119–126.

62 G. Nazri, Preparation, structure and ionic conductivity of lithium phosphide, *Solid State Ionics*, 1989, **34**, 97–102.

63 S. P. Jand, Q. Zhang and P. Kaghazchi, Theoretical study of superionic phase transition in Li_2S, *Sci. Rep.*, 2017, **7**, 5873.

64 A. Sohib, M. A. Irham, J. Karunawan, S. P. Santosa, O. Floweri and F. Iskandar, Interface analysis of LiCl as a protective layer of $Li_{1.3}Al_{0.3}Ti_{1.7}(PO_4)_3$ for electrochemically stabilized all-solid-state Li-metal batteries, *ACS Appl. Mater. Interfaces*, 2023, **15**(13), 16562–16570.

65 X. Wu, Y. Gong, S. Xu, Z. Yan, X. Zhang and S. Yang, Electrical conductivity of lithium chloride, lithium bromide, and lithium iodide electrolytes in methanol, water, and their binary mixtures, *J. Chem. Eng. Data*, 2019, **64**(10), 4319–4329.

66 O. Nakamura and J. B. Goodenough, Conductivity enhancement of lithium bromide monohydrate by Al_2O_3 particles, *Solid State Ionics*, 1982, **7**(2), 119–123.

67 M. Armand, P. Axmann, D. Bresser, M. Copley, K. Edström, C. Ekberg, D. Guyomard, B. Lestriez, P. Novák, M. Petranikova, W. Porcher, S. Trabesinger, M. Wohlfahrt-Mehrens and H. Zhang, Lithium-ion batteries – Current state of the art and anticipated developments, *J. Power Sources*, 2020, **479**, 228708.

68 M. Duclot and J.-L. Souquet, Glassy materials for lithium batteries: electrochemical properties and devices performances, *J. Power Sources*, 2001, **97–98**, 610–615.

69 C. Julien and G. A. Nazri, *Solid state batteries: Materials design and optimization*, Kluwer Academic Publishers, Boston (1994).

70 N. J. Dudney, Solid-state thin-film rechargeable batteries, *Mater. Sci. Eng. B*, 2005, **116**, 245–249.

71 S. Lim, K. Lee, I. Shin, A. Tron, J. Mun, T. Yim and T.-H. Kim, Physically cross-linked polymer binder based on poly(acrylic acid) and ion-conducting poly(ethylene glycol-*co*-benzimidazole) for silicon anodes, *J. Power Sources*, 2017, **360**, 585–592.

72 E.-L. Zhao, S.-X. Zhao, X. Wu, J.-W. Li, L.-Q. Yu, C.-W. Nan and G. Cao, Electrochemical performance of Li_2O–V_2O_5–SiO_2–B_2O_3 glass as cathode material for lithium ion batteries, *J. Materiomics*, 2019, **5**, 663–669.

73 S. H. Choi, S. J. Lee, H. J. Kim, S. B. Park and J. W. Choi, Li_2O–B_2O_3–GeO_2 glass as a high performance anode material for rechargeable lithium-ion batteries, *J. Mater. Chem. A*, 2018, **6**, 6860.